applied optics

1200°C high-temperature distributed optical fiber sensing using Brillouin optical time domain analysis

Pengbai Xu,[1] Yongkang Dong,[1,*] Dengwang Zhou,[1] Cheng Fu,[1] Juwang Zhang,[1] Hongying Zhang,[2] Zhiwei Lu,[1,4] Liang Chen,[3] and Xiaoyi Bao[3]

[1]National Key Laboratory of Science and Technology on Tunable Lasers, Harbin Institute of Technology, Harbin 150001, China
[2]Institute of Photonics and Optical Fiber Technology, Harbin University of Science and Technology, Harbin 150080, China
[3]Fiber Optics Group, Department of Physics, University of Ottawa, Ottawa K1N 6N5, Canada
[4]e-mail: lvzw@hit.edu.cn
*Corresponding author: aldendong@gmail.com

Received 12 May 2016; revised 13 June 2016; accepted 13 June 2016; posted 14 June 2016 (Doc. ID 264997); published 12 July 2016

In this paper, up to 1100°C and 1200°C high-temperature distributed Brillouin sensing based on a GeO_2-doped single-mode fiber (SMF) and a pure silica photonic crystal fiber (PCF) are demonstrated, respectively. The Brillouin frequency shift's (BFS) dependence on temperatures of the SMF and PCF agrees with a nonlinear function instead of a linear function, which is mainly due to the change of the acoustic velocity in a silica fiber. BFS hopping is observed in both kinds of fibers between 800°C–900°C in the first annealing process, and after that, the BFS exhibits stability and repeatability with a measurement accuracy as high as ±2.4°C for the SMF and ±3.6°C for the PCF. The BFS hopping is a highly temperature-dependent behavior, which means that a high temperature (>800°C) would accelerate this process to reach a stable state. After BFS hopping, both the SMF and PCF show good repeatability for temperatures higher than 1000°C without annealing. The process of coating burning of a silica fiber not only introduces a loss induced by micro-bending, but also imposes a compressive stress on the bare fiber, which contributes to an additional BFS variation at the temperature period of the coating burning (~300°C–500°C).

OCIS codes: (290.5900) Scattering, stimulated Brillouin; (060.5295) Photonic crystal fibers; (280.6780) Temperature.

http://dx.doi.org/10.1364/AO.55.005471

1. INTRODUCTION

Stimulated Brillouin scattering (SBS) used as an effective sensing mechanism has been widely reported over the past twenty years [1,2]. A so-called truly distributed sensing technique named the Brillouin optical time domain analysis (BOTDA) has been widely developed due to its advantages of a high signal-to-noise ratio (SNR) and high accuracy [3–5]. Currently, the development of the BOTDA technique includes two perspectives: the development of a new BOTDA-based sensing scheme [6–10], and the development of new-type optical fibers for stimulated Brillouin scattering [11–16]. The new schemes include a pulse coding technique [6], a Raman-assisted amplifying technique [7], a differential pulse-width pair technique [8], a pre-pump-pulse technique [9], and a dynamic BOTDA technique [10], which could effectively extend the sensing range, improve the spatial resolution, and shorten the measuring time for strain/temperature sensing purposes. New-type fiber-based sensors include polymer optical fibers for large-scale strain sensing [11,12], few-mode fibers or polarization-maintaining optical fibers for multiple parameter sensing [13,14], multimode optical fibers with excited fundamental modes for bend-insensitive sensing [15], and silica microwires for highly nonlinear applications [16], which could further extend the application scope of the BOTDA technique.

One of these applications is high-temperature monitoring, which is one of the major concerns in the processes of controlling and machining, such as in heavy energy-consuming industries [17] or volcanic events [18]. Up to now, a large number of discrete fiber-optic high-temperature sensors have been developed [19–24] that feature compact size and instantaneity. The difficulty of multiplexing is a huge challenge to achieve distributed high-temperature sensing. Therefore, it is highly desirable to develop a distributed high-temperature fiber sensor that features low cost, high reliability, and high accuracy. An early work of Thévenaz characterized the Brillouin gain spectrum of a single-mode fiber (SMF) from −272°C to 727°C and revealed the nonlinear relationship between the Brillouin frequency shift (BFS) and temperature [25]. Reference [26] investigated the

temperature dependence of the (BFS) in a commercially available dispersion-shifted fiber in the range of 20°C–820°C, although distributed-fiber high-temperature sensing was not achieved in their study. Although Ref. [27] demonstrated that 1000°C high-temperature distributed sensing can be achieved with the BOTDA technique in an SMF, it was not a systematic investigation that could offer insight into the nature of high-temperature distributed sensing, and several significant problems have not been illustrated.

In this paper, we demonstrate an up to 1100°C and 1200°C high-temperature distributed Brillouin sensing based on a GeO_2-doped SMF and a pure silica photonics crystal fiber (PCF). BFS hopping is observed in both kinds of fibers between 800°C–900°C in the first annealing process, and after that, the BFS exhibits stability and repeatability with a measurement accuracy as high as ±2.4°C for the SMF and ±3.6°C for the PCF. For temperature measurements >1000°C, the annealing process is not required for both fibers since the BFS is same in this temperature, including during the first-time measurement. The process of coating burning of the fiber not only introduces a loss induced by micro-bending, but also imposes a compressive stress on the bare fiber, which contributes to an additional BFS variation at the temperature period of the coating burning (~300°C to 500°C). The BFS dependence on the high temperatures of the SMF and PCF is a nonlinear function instead of a linear function, which is mainly due to the change of the acoustic velocity in a silica fiber.

Compared with the discrete fiber-optic high-temperature sensors [23,24] that need to be annealed several times to achieve an adequate stable functionality level, the distributed Brillouin optical fiber sensors (including the SMF and PCF) only need to be annealed one time to reach a reliable level for practical use, which makes them more convenient for high-temperature measurements.

2. PRINCIPLE

When light travels in the fiber, a backscattered light called Stokes light is generated due to the acoustic waves (phonons) excited by the electrostriction mechanism, which is known as spontaneous Brillouin scattering. The backscattered Stokes light suffers a Doppler shift called the Brillouin frequency shift, which is given by [28]

$$\nu_B = \frac{2n_{\text{eff}}v_A}{\lambda_P}, \tag{1}$$

where n_{eff} is the effective core refractive index, v_A is the acoustic velocity, and λ_P is the wavelength of the pump wave in a vacuum. If the frequency of the introduced downshifted probe wave equals the frequency of the Stokes wave, stimulated Brillouin scattering (SBS) would occur and the higher-frequency pump would convert part of its energy to the lower-frequency probe through the acoustic wave field. The BOTDA technique incorporates the SBS process and the optical time domain analysis technique, which uses pulse light as the pump and frequency downshifted continuous light as the probe and features high sensing accuracy and long sensing distances [5,29].

3. EXPERIMENTAL SETUP

The experimental setup is illustrated in Fig. 1. The output of an optical fiber laser is divided into two arms by a 50/50 coupler providing two waves, i.e., a pump and a probe. An arbitrary function generator is used to drive a high extinction ratio (>45 dB) electro-optic modulator (EOM) to generate the pump pulse. A polarization scrambler is used to randomly change the polarization state of the pump pulse to reduce polarization fading-induced fluctuations in the signal by averaging a large number of signal traces. We used 1000 times averaging in our experiment. The pump pulse is amplified by an erbium-doped fiber amplifier and then sent into the fiber under test (FUT). The continuous probe beam is modulated by another EOM, which is driven by a microwave generator to generate carrier-suppressed two-sideband modulation by adjusting the bias voltage of the modulator. Two beams interact in the FUT, and the SBS interaction occurs. The Brillouin signal is extracted by a filter and converted into an electrical signal with a photo detector and monitored by an oscilloscope, and then a BGS can be obtained by changing the probe frequency at a step of 4 MHz in the vicinity of the BFS. The FUT includes a 2 m PCF (NKT photonics, LMA-10) and a 50 m SMF (Yangtze Ltd.). Note that the width of the pump pulse used in the experiment is 10 ns, corresponding to a 1 m spatial resolution in a silica fiber. The peak power of the pulsed pump is ~400 mW and the power of the probe is ~1 mW, which lead to a relative high signal intensity. The high-temperature measurements for the SMF and PCF are achieved with a chamber furnace (Chinese Academy of Science Instrument Department, SXL-1400C), of which the temperature is monitored by an electrical thermocoupler with a measuring accuracy of ±1°C.

4. EXPERIMENTAL RESULTS

A. SMF for 1100°C High-Temperature Distributed Sensing

First, an SMF is used to measure the high temperatures. A ~2.4 m fiber section located at the end of a 50 m SMF is put into the chamber furnace, and the temperature is increased in steps of 100°C. The distributed measurement results are shown in Fig. 2(a). It is shown that the BFS of the SMF

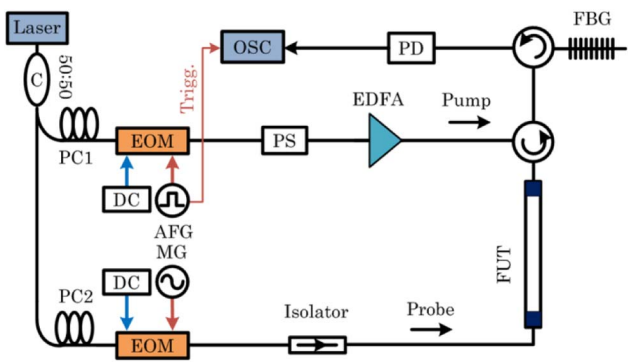

Fig. 1. Experimental setup. C, coupler; PC, polarization controller; EOM, electro-optic modulator; DC, direct current; AFG, arbitrary function generator; MG, microwave generator; PS, polarization scrambler; EDFA, erbium-doped fiber amplifier; FUT, fiber under test; FBG, fiber Bragg grating; PD, photo detector; OSC, oscilloscope.

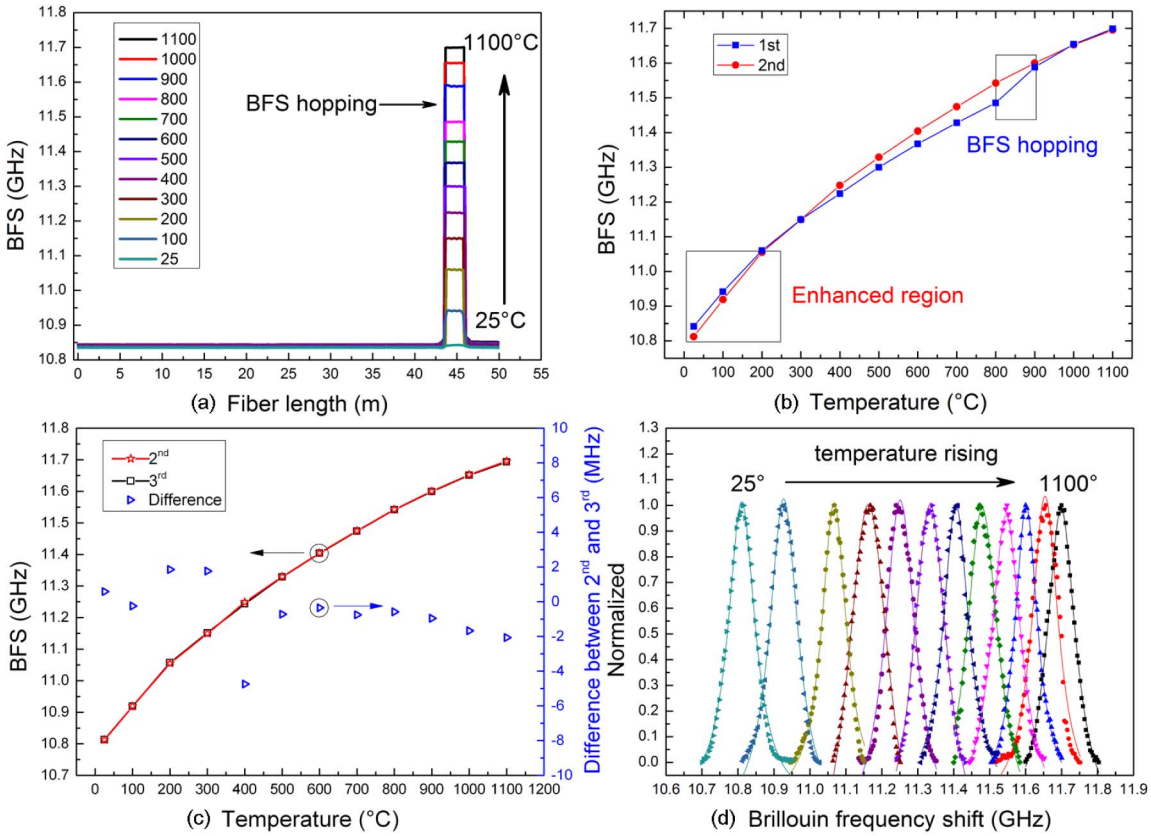

Fig. 2. Measurement results of SMF in the range of 25°C–1100°C, (a) measured Brillouin frequency shifts over a 50 m-long sensing fiber, where the BFS hopping is observed between 800°C–900°C, (b) the comparison of first and second measurements, where the BFS hopping disappears for the second measurement, (c) the comparison of the second and third measurements and their difference, and (d) measured Brillouin gain spectra in the range of 25°C–1100°C after the first annealing.

increases nonlinearly from 25°C to 1100°C and there is a big BFS increase, called "BFS hopping," between 800°C and 900°C, which can be clearly observed in the blue curve of Fig. 2(b). After the first measurement up to 1100°C, the chamber furnace is programmatically controlled and cooled down to room temperature in 10 h, and then a second measurement is conducted. The results of the first and second measurements are shown in Fig. 2(b), where the BFS variation of the heated fiber still increases nonlinearly, while the BFS hopping has disappeared. This phenomenon is mainly due to the internal stress of the glass accumulated when the fiber was drawing [30], and it can be eliminated by a first-time heating called "annealing." In Fig. 2(b), in the range of 25°C–200°C, the temperature coefficient is 1.246 MHz/°C in the first annealing process and 1.387 MHz/°C in the second measurement, which shows a ~11.3% temperature coefficient enhancement. In order to be sure that the fiber is stable and reproducible for the practical use, a third measurement is conducted, and a comparison of the second and third measurements is shown in Fig. 2(c), where the two curves coincide pretty well. The difference between the second and third measurements is shown at the right axis of Fig. 2(c), which is within ±2 MHz except for 400°C, which is probably due to the temperature fluctuation of the chamber furnace. The BFS of the SMF changes with the temperature nonlinearly instead of linearly, which coincides with the results in Ref. [26]. The BGSs of the SMF from 25°C to 1100°C are shown in Fig. 2(d), where the solid lines show Lorentzian fits that are in good accordance with the Lorentzian function.

B. Characterization of BFS Hopping

Next, the "BFS hopping" between 800°C and 900°C is investigated, and the results are shown in Fig. 3(a). A 10 m SMF section is put into the chamber furnace and the temperature is kept at 800°C, 850°C, and 900°C for 2 h. Every 50°C increment of the temperature needs 20 min to reach a stable temperature field in the chamber furnace. The BFS is measured and shown as the black square points in Fig. 3(a), and the red round points show the BFS difference between every two adjacent points (d_{BFS}) at each period. At the period of 800°C, the fiber remains at a stable level and the BFS shows almost no changes within 2 h, which indicates that the BFS hopping does not vary obviously at this temperature [30]. Next, the chamber furnace is heated to 850°C in 20 min, and the BFS increases considerably during the first 40 min and then the growth rate slows down, which indicates that the "BFS hopping" is evident at this temperature. When the temperature is increased to 900°C, the BFS shifts very slowly, and thus the "BFS hopping" reaches a relatively stable level. In Fig. 2(b), note that the BFSs coincide pretty well between the first and second measurements from 1000°C to 1100°C, which indicates that the "BFS hopping"

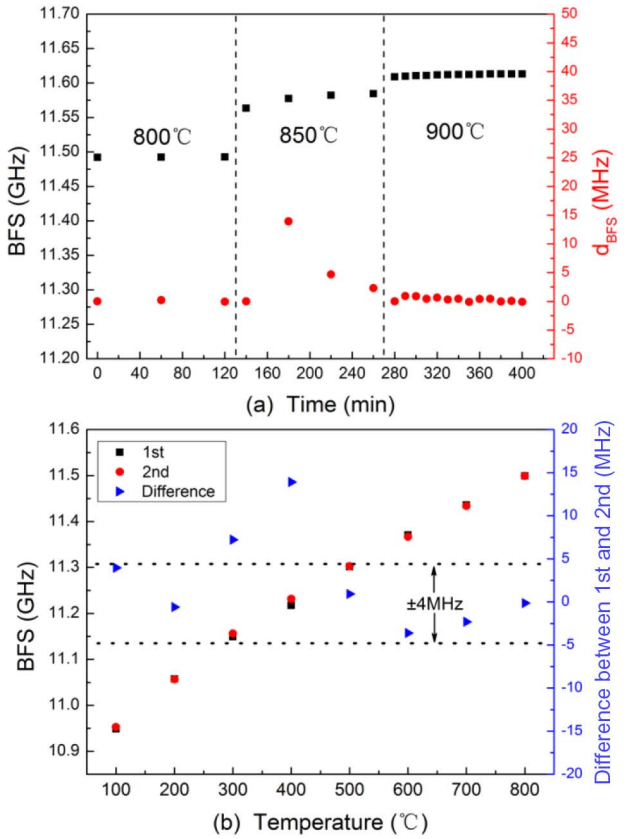

Fig. 3. (a) Investigations on BFS hopping. The BFSs are shown as black square points, and the red round points are the BFS difference between every two adjacent points at each period (d_{BFS}). (b) Comparison of two measurements under temperature region of BFS hopping.

was done before 1000°C, so temperature sensing above 1000°C can be done without the first annealing. Therefore, the "BFS hopping" is a highly temperature-dependent behavior, which indicates that the time of releasing the internal stress is related to the temperature.

In what follows, the stability of the SMF is investigated before the emergence of the BFS hopping behavior, i.e., from 100°C to 800°C. As illustrated in Fig. 3(b), the two measurements are conducted, and the BFS differences between the first and second measurements are shown at the right axis. The two measurements generally match well and the BFS difference is no more than ±4 MHz except for 300°C and 400°C (7.2 and 13 MHz difference), which is probably caused by the coating of the fiber.

C. Characterization of Coating Burning

Next, the effect of the coating (composition: double-layer acrylate, thickness: 125 μm) is investigated by making a comparison between a coated and uncoated fiber. Two pieces of 2 m fiber sections (one has a coating and the other's coating is purposely stripped off) are put into the chamber furnace together, and the temperature is increased from 25°C to 1100°C. The results are shown in Fig. 4(a). The left axis shows the BFS variation, and the right axis shows the BFS differences between the two

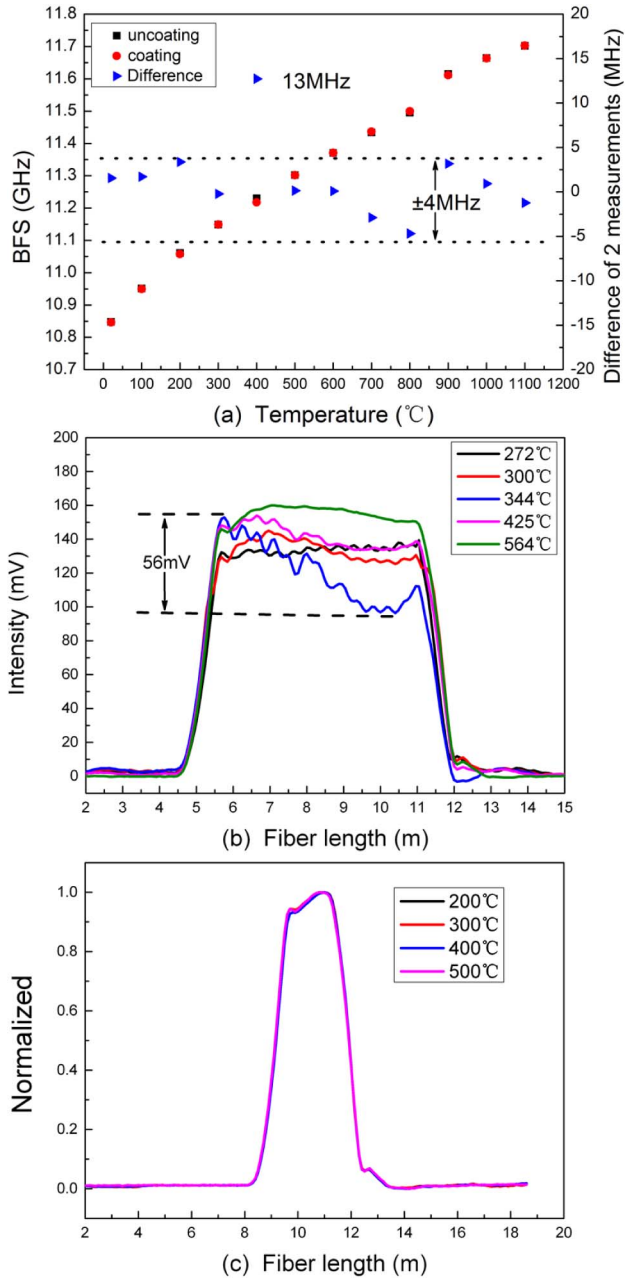

Fig. 4. (a) Influence of coating burning on the bare SMF. (b) BOTDA time traces at 272°C, 344°C, and 564°C with coating. (c) BOTDA time traces at 200°C, 300°C, 400°C, and 500°C without coating.

measurements. The difference is no more than ±4 MHz except for 400°C, at which degree the BFS of the uncoated fiber is 13 MHz larger than that of the coated fiber. This is the same result as in Fig. 3(b); the difference is that the coating of the fiber is not stripped off. Hence, the big BFS difference at 400°C is probably due to the coating burning.

To further investigate this problem, we checked the BOTDA time traces from 25°C to 600°C continuously, which is the temperature region of the coating burning. The results are shown in Fig. 4(b). At 272°C, the BOTDA time trace shows no

loss. The periodic fluctuations in the signal could result from the coating pyrolysis, which induced an additional stress on the fiber and the temperature non-uniformity inside chamber furnace. Then, the loss in the signal enlarges as the temperature gradually increases, as shown in the red curve of 300°C. At 344°C, the signal experiences a maximum loss of 36.8% (56 mV), which can be clearly seen on the blue curve. The signal loss is mainly due to the stress accumulated on the fiber-produced micro-bending [31]. After that, the loss starts to reduce and the signal begins to recover, which indicates that the coating burning-induced stress on the bare fiber is smaller and smaller, as shown in the pink curve of 425°C. At 564°C, the signal is smooth again and enhanced compared to the former ones, which shows that the coating has been burned out. These results indicate that the coating burning would introduce an inevitable loss, which would to some degree introduce a fitting error to the Brillouin signal. In addition, the coating burning-induced compressive stress would further lead to a BFS shift, which also contributes to the BFS difference at the temperature period of the coating burning. Last, we also check the BOTDA time traces of the uncoated fiber, where the data was extracted from Fig. 4(a) at 200°C, 300°C, 400°C, 500°C and was normalized so as to cancel the power variations of the pump and probe. It can be seen clearly that, in Fig. 4(c), there is no loss on the bare fiber for each signal, which confirms that the observed loss in Fig. 4(b) is due to coating burning.

D. PCF for 1200°C High-Temperature Distributed Sensing

Then, the PCF for high-temperature measurements is conducted. The sensing fiber is made up of a ~2 m total internal reflection type of PCF and two pieces of SMF spliced at the both ends of the PCF, and its total length is 12 m. The distributed measurement results are shown in Fig. 5(a). An up to 1200°C temperature is applied to the PCF in steps of 100°C, the BFS increases with the temperature nonlinearly, and there is still BFS hopping between 800°C and 900°C, as with the SMF. In Fig. 5(b), the BFS hopping has disappeared after annealing. In the first annealing process, the temperature coefficient of the PCF is 1.18 MHz/°C from 26°C to 200°C, and in the second measurement, it is 1.42 MHz/°C from 36°C to 200°C, which shows that the temperature coefficient of ~20.3% has been improved. This enhanced temperature coefficient could be due to the internal stress release when the fiber was drawing. What is more, the PCF shows good repeatability between the first and second measurements from 1000°C to 1200°C, which indicates that it can work effectively in this temperature range without annealing. In Fig. 5(c), the comparison of the second and third measurements shows that the PCF has good repeatability. The difference of the second and third measurements is shown at the right axis of Fig. 5(c). The maximum temperature uncertainty is ±4 MHz except for 300°C and 400°C, which is probably due to the temperature fluctuation of the chamber furnace. The BFS of the PCF changes with the temperature nonlinearly,

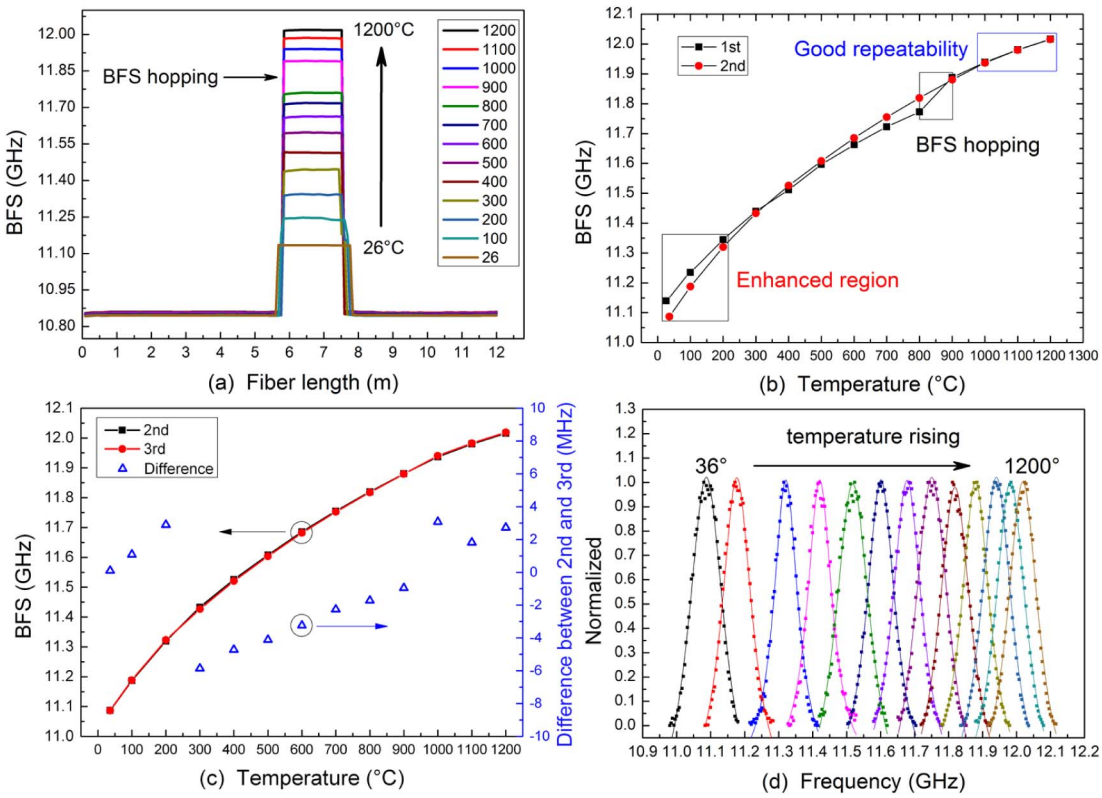

Fig. 5. Measurement results of PCF in the range of 36°C–1200°C, (a) distributed measurements of Brillouin frequency shifts over the sensing fiber, where the Brillouin frequency shift hopping is observed between 800°C–900°C, (b) the comparison of the first and second measurements, where the BFS hopping disappears for the second measurement, (c) the comparison of the second and thirdmeasurements and their difference, and (d) measured Brillouin gain spectra in the range of 36°C–1200°C, after the first annealing.

which is the same as with the SMF. As mentioned above, the BFS is determined by Eq. (1). The temperature coefficient of the effective index is about $1 \times 10^{-5}/°C$ [32], which is much lower than that of the BFS, whose average coefficient is $7.19 \times 10^{-5}/°C$, calculated from $(dv_B/dT)/v_{B0}$ (v_{B0} is the BFS at room temperature) in the temperature range of 36°C to 1200°C and depicted in Fig. 5(c). Therefore, the origin of the nonlinear BFS dependence on the temperature is mainly due to the velocity variations of the acoustic wave [33]. More specifically, there is a nonlinear relationship between the modulus and temperature [34], which shows that the nonlinear BFS behavior with temperature could be due to the silica material's behavior. Figure 5(d) shows the BGSs of the PCF, and the solid lines show Lorentzian fits. Here, we should note that the different linewidths in Fig. 5(d) as well as in Fig. 2(d) are mainly due to the temperature fluctuation and inhomogeneous distribution in the chamber furnace. We use a 10 ns pump pulse corresponding to a ~100 MHz BGS linewidth, while the period of the BGS measurement is several minutes, at which the temperature of the chamber furnace would go up and down periodically, especially under 600°C, both of which would inevitably induce the linewidth of BGS to broaden.

E. Effect of Coating Burning on the PCF

Based on the analysis of the coating burning effect on the SMF, we analyze the effect of the coating burning on the PCF by comparing two measurements from 100°C to 800°C. Different from the coating of the SMF, which is easy to strip for several meters, the coating (composition: single-layer acrylate, thickness: 125 μm) of the PCF is so hard to strip off that any further stress imposed on the bare PCF would break it. Thus, we put 1 m PCF section with a coating into the chamber furnace and measure it twice to analyze the coating burning effect.

As shown in Fig. 6, the round black points show the BFSs of the first measurement with coating, the red square points are the BFSs of the second measurement when the coating has been burned, and the blue triangle points represent the BFS difference between the two measurements. Unlike the results of the SMF in Fig. 3(b), the BFSs of the second measurement are between 15–27 MHz lower than that of the first measurement from 100°C to 700°C, which indicates that the coating would introduce a tensile stress when the fiber was drawing. At the coating burning period around 400°C, the BFS difference is smaller than that of 300°C and 600°C, which indicates that coating burning introduced an additional compressive stress that counteracts the tensile stress of fiber drawing. This phenomenon can also be clearly observed in Fig. 5(a): the BFS difference of 69 MHz between 300°C and 400°C is clearly smaller than the BFS difference of 83 MHz between 400°C and 500°C, which indicates that the BFS at 400°C has been reduced by coating burning-induced compressive stress. These results of the coating effect on the PCF coincide with those of the SMF in that an additional compressive stress is produced on the bare fiber during this period.

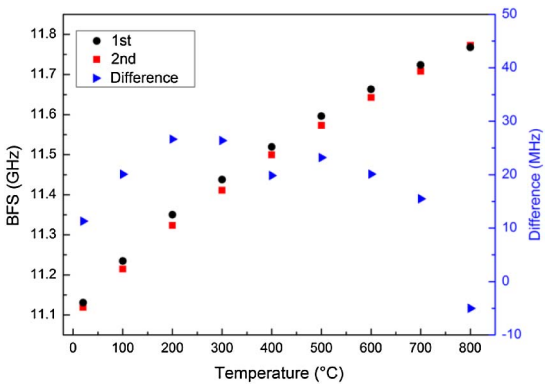

Fig. 6. Influence of coating burning on the bare PCF.

5. DISCUSSION

At the temperature of 1100°C, the SMF is kept for 32 h and there is no additional loss produced, which indicates that the fiber could measure temperatures as high as 1100°C reliably and stably for a long time. However, the loss of the SMF is instantly increased when the chamber furnace reaches 1200°C, which is mainly due to the dopant diffusion of the core that modifies its guiding property and fiber devitrification, i.e., the growth of a crystalline structure substituting the amorphous structure of the glass [35]. In the case of the PCF that is made of pure silica with a regular hexagonal lattice, the fact that it can work at a higher temperature is mainly due to the exclusion of dopant diffusion. Actually, we indeed use the PCF to achieve distributed fiber sensing as high as 1200°C. However, the PCF could be only kept in the chamber furnace for ~3 h at 1200°C, and then a significant loss of about 2.4 dB/m is produced, which indicates that the fiber structure has been destroyed gradually. Figure 7(a) shows the loss of the PCF increases with time at 1200°C, and after it produces 2.4 dB/m, the loss increases quickly in 2 h. Since there is no dopant in the core of the PCF, the reason for the loss is due to fiber devitrification. For a pure silica PCF with a regular arrangement of air holes to form its waveguide structure, a 1200°C temperature would make the fiber fracture as polycrystalline structures form [25,35] and undergo a transition process [34], which would produce cracks on the fiber and hence contribute to a continuous loss. Figure 7(b) shows the temperature coefficients of the PCF and SMF at 100°C. We can see that both fibers' temperature coefficients decrease gradually with the temperature, while the PCF's temperature coefficient shows a larger variation range than that of the SMF. Compared with the SMF, the PCF's temperature coefficient is larger before 900°C, while after 900°C, the PCF's temperature coefficient is smaller, which makes it easier for the PCF to produce a larger sensing uncertainty than the SMF at >900°C.

In addition, scanning electron microscope (SEM) micrographs for the cross sections of the PCF before and after annealing are acquired, as shown in Fig. 8. The diameter d of the air holes and the pitch Λ of the lattice at room temperature are ~2.89 and ~6.5 μm, respectively. After annealing at 1200°C for 5 h, the diameter of the air holes is 2.42 μm, while the pitch of lattice is still 6.5 μm, which indicates that the air holes of the PCF have collapsed by 14.5%. This phenomenon would lead to some extent to the expansion of the mode field area of the PCF, which would be easily influenced by the cracks

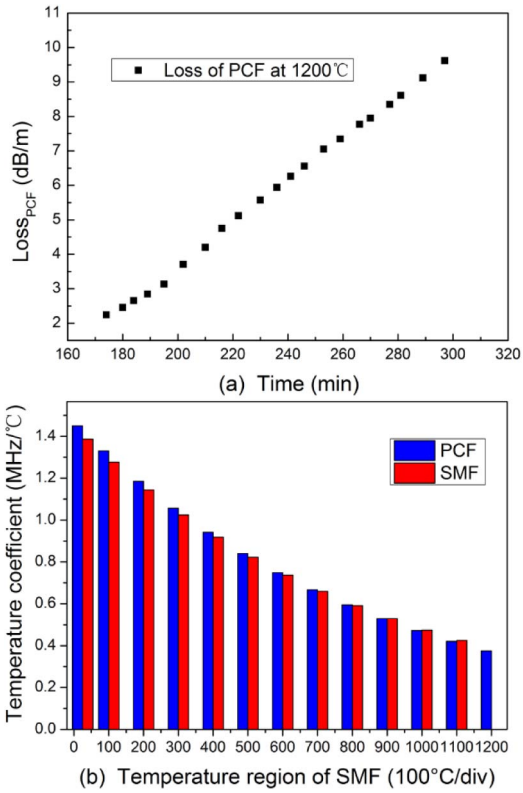

Fig. 7. (a) The loss of PCF at 1200°C in 5 h, and (b) the comparison of the temperature coefficients between the PCF and SMF at 100°C.

induced by fiber devitrification and would further increase the light scattering, hence producing an extra loss.

Last, we analyze the measurement accuracy of the SMF and PCF by acquiring the temperature coefficients of the BFS at 100°C, and get the BFS difference between the second and third measurements at 100°C in Figs. 2(c) and 5(c) as the BFS uncertainty. By calculating the temperature uncertainty from the BFS uncertainty and temperature coefficient, the maximum temperature uncertainty is ±2.4°C for the SMF at 1100°C and ±3.6°C at 1200°C for the PCF, including the accuracy of the chamber furnace of ±1°C.

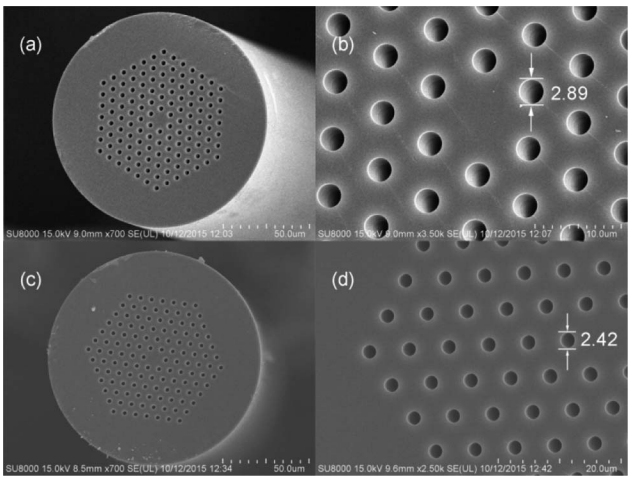

Fig. 8. SEM of PCF, (a) normal end face of PCF at room temperature, (b) micrograph around the core, $d = \sim 2.89$ μm, $A = \sim 6.5$ μm, (c) after annealing at 1200°C for 5 h, and (d) micrograph on one side of the core, $d = \sim 2.42$ μm, $A = \sim 6.5$ μm.

6. CONCLUSION

In conclusion, we demonstrate up to 1100°C and 1200°C high-temperature distributed Brillouin sensing based on a GeO_2-doped SMF and a pure silica PCF. BFS hopping is observed in both kinds of fibers between 800°C–900°C in the first annealing process, and after that, the BFS exhibits stability and repeatability with a measurement accuracy as high as ±2.4°C for the SMF and ±3.6°C for the PCF. This BFS hopping is a highly temperature-dependent behavior, which means that a higher temperature would accelerate the process of BFS hopping to reach a stable functional level. After the first annealing, the temperature coefficient has been improved by ~11.3% and ~20.3% from room temperature to 200°C for the SMF and PCF, respectively, which could be due to the internal stress release. For temperature measurements >1000°C, the annealing process is not required for the fibers since the BFS is same in this temperature, including the first-time measurement. The process of coating burning of the fiber not only introduces a loss induced by micro-bending, but also imposes a compressive stress on the bare fiber, which contributes to the BFS variations at the temperature period of coating burning (~300°C to 500°C). The observed phenomenon of BFS hopping and the effect of coating burning turn out to be detrimental for distributed high-temperature sensing and can be eliminated in a first-time annealing. The BFS dependence on high temperatures of SMFs and PCFs is a nonlinear function instead of a linear function, which is mainly due to the change of the acoustic velocity in a silica fiber. The PCF could measure 1200°C for short times (in first 3 h), and it is stable and reliable after one-time annealing. Although the PCF would produce a huge loss at 1200°C after 3 h and start to fail in the measurement, it is still meaningful and could be qualified for 1200°C high-temperature distributed sensing, temperatures at which SMFs are not competent.

From a user's point of view, it is recommended to use the fiber directly when the measured temperature is less than 200°C; due to the impacts of coating burning and BFS hopping, it is strongly recommended to perform the first-time annealing process for the fiber when the temperature is higher than 200°C, where the annealing process usually needs several hours at a temperature higher than 850°C. In practical use, in order for these two fibers to achieve high-temperature sensing, it is best to coat them with a metal coating, which can effectively protect the fibers, since the silica fiber is fragile after annealing, and can effectively couple the outer temperature field to the inner fibers.

Funding. 863 Program of China (2014AA110401); National Key Technology Research and Development Program of the Ministry of Science and Technology of China (2014BAG05B07); National Key Scientific Instrument and Equipment Development Project (2013YQ040815);

National Natural Science Foundation of China (NSFC) (61575052, 61308004); Scientific Research Fund of Heilongjiang Provincial Education Department (12531093, ZD201415).

REFERENCES

1. E. P. Ippen and R. H. Stolen, "Stimulated Brillouin scattering in optical fibers," Appl. Phys. Lett. **21**, 539–541 (1972).
2. Y. Mizuno and K. Nakamura, "Experimental study of Brillouin scattering in perfluorinated polymer optical fiber at telecommunication wavelength," Appl. Phys. Lett. **97**, 021103 (2010).
3. T. Horiguchi and M. Tateda, "Optical-fiber-attenuation investigation using stimulated Brillouin scattering between a pulse and a continuous wave," Opt. Lett. **14**, 408–410 (1989).
4. Y. Dong, L. Chen, and X. Bao, "Time-division multiplexing-based BOTDA over 100 km sensing length," Opt. Lett. **36**, 277–279 (2011).
5. Y. Dong, H. Zhang, L. Chen, and X. Bao, "2 cm spatial-resolution and 2 km range Brillouin optical fiber sensor using a transient differential pulse pair," Appl. Opt. **51**, 1229–1235 (2012).
6. M. A. Soto, G. Bolognini, F. D. Pasquale, and L. Thévenaz, "Simplex-coded BOTDA fiber sensor with 1 m spatial resolution over a 50 km range," Opt. Lett. **35**, 259–261 (2010).
7. F. Rodríguez-Barrios, S. Martín-López, A. Carrasco-Sanz, P. Corredera, J. Ania-Castañón, L. Thévenaz, and M. González-Herráez, "Distributed Brillouin fiber sensor assisted by first-order Raman amplification," J. Lightwave Technol. **28**, 2162–2172 (2010).
8. W. Li, X. Bao, Y. Li, and L. Chen, "Differential pulse-width pair BOTDA for high spatial resolution sensing," Opt. Express **16**, 21616–21625 (2008).
9. K. Kishida, L. CheHiena, and K. Nishiguchi, "Pulse pre-pump method for cm-order spatial resolution of BOTDA," in *17th International Conference on Optical Fiber Sensors*, Bellingham, WA, 2005, Vol. **5855**.
10. Y. Dong, D. Ba, T. Jiang, D. Zhou, H. Zhang, C. Zhu, Z. Lu, H. Li, L. Chen, and X. Bao, "High-spatial-resolution fast BOTDA for dynamic strain measurement based on differential double-pulse and second-order sideband of modulation," IEEE Photon. J. **5**, 2600407 (2013).
11. N. Hayashi, Y. Mizuno, and K. Nakamura, "Brillouin gain spectrum dependence on large strain in perfluorinated graded-index polymer optical fiber," Opt. Express **20**, 21101–21106 (2012).
12. Y. Dong, P. Xu, H. Zhang, Z. Lu, L. Chen, and X. Bao, "Characterization of evolution of mode coupling in a graded-index polymer optical fiber by using Brillouin optical time-domain analysis," Opt. Express **22**, 26510–21106 (2014).
13. A. Li, Y. Wang, J. Fang, M. Li, B. Y. Kim, and W. Shieh, "Few-mode fiber multi-parameter sensor with distributed temperature and strain discrimination," Opt. Lett. **40**, 1488–1491 (2015).
14. Y. Dong, L. Chen, and X. Bao, "High-spatial-resolution time-domain simultaneous strain and temperature sensor using Brillouin scattering and birefringence in a polarization-maintaining fiber," IEEE Photon. Technol. Lett. **22**, 1364–1366 (2010).
15. P. Xu, Y. Dong, J. Zhang, D. Zhou, T. Jiang, J. Xu, H. Zhang, T. Zhu, Z. Lu, L. Chen, and X. Bao, "Bend-insensitive distributed sensing in singlemode-multimode-singlemode optical fiber structure by using Brillouin optical time-domain analysis," Opt. Express **23**, 22714–22722 (2015).
16. J. Beugnot, S. Lebrun, G. Pauliat, H. Maillotte, V. Laude, and T. Sylvestre, "Brillouin light scattering from surface acoustic waves in a subwavelength-diameter optical fibre," Nat. Commun. **5**, 5242 (2014).
17. T. L. Lowder, K. H. Smith, B. L. Ipson, A. R. Hawkins, R. H. Selfridge, and S. M. Schultz, "High-temperature sensing using surface relief fiber Bragg gratings," IEEE Photon. Technol. Lett. **17**, 1926–1928 (2005).
18. T. Zhu, T. Ke, Y. Rao, and K. S. Chiang, "Fabry–Perot optical fiber tip sensor for high temperature measurement," Opt. Commun. **283**, 3683–3685 (2010).
19. D. Monzón-Hernández, V. P. Minkovich, and J. Villatoro, "High-temperature sensing with tapers made of microstructured optical fiber," IEEE Photon. Technol. Lett. **18**, 511–513 (2006).
20. L. Xu, M. Deng, D. Duan, W. Wen, and M. Han, "High-temperature measurement by using a PCF-based Fabry–Perot interferometer," Opt. Lasers Eng. **50**, 1391–1396 (2012).
21. J. E. Antonio-Lopez, Z. S. Eznaveh, P. LiKamWa, A. Schülzgen, and R. Amezcua-Correa, "Multicore fiber sensor for high-temperature applications up to 1000°C," Opt. Lett. **39**, 4309–4312 (2014).
22. A. V. Newkirk, E. Antonio-Lopez, G. Salceda-Delgado, R. Amezcua-Correa, and A. Schülzgen, "Optimization of multicore fiber for high-temperature sensing," Opt. Lett. **39**, 4812–4815 (2014).
23. Q. Rong, X. Qiao, T. Guo, H. Yang, Y. Du, D. Su, R. Wang, H. Sun, D. Feng, and M. Hu, "High temperature measurement up to 1100°C using a polarization-maintaining photonic crystal fiber," IEEE Photon. J. **6**, 6800309 (2014).
24. G. Coviello, V. Finazzi, J. Villatoro, and V. Pruneri, "Thermally stabilized PCF-based sensor for temperature measurements up to 1000°C," Opt. Express **17**, 21551–21559 (2009).
25. L. Thévenaz, A. Fellay, and W. Scandale, "Brillouin gain spectrum characterization in optical fibres from 1 to 1000 K," in *16th International Conference on Optical Fiber Sensors* (IECE, 2003), paper Tu2-2.
26. Y. Li, F. Zhang, and T. Yoshino, "Wide-range temperature dependence of Brillouin shift in a dispersion-shifted fiber and its annealing effect," J. Lightwave Technol. **21**, 1663–1667 (2003).
27. J. Wang, D. Hu, Y. D. Wang, and A. Wang, "Fully-distributed fiber-optic high temperature sensing based on stimulated Brillouin scattering," in *Proceedings of 17th International Conference on Optical Fiber Sensors and Applications X*, Baltimore, MD (2013), Vol. **8722**.
28. G. P. Agrawal, *Nonlinear Fiber Optics* (Academic, 1995).
29. Y. Dong, L. Chen, and X. Bao, "Extending the sensing range of Brillouin optical time-domain analysis combining frequency-division multiplexing and in-line EDFAs," J. Lightwave Technol. **30**, 1161–1167 (2012).
30. Y. Mohanna, J. Saugrain, J. Rousseau, and P. Ledoux, "Relaxation of internal stresses in optical fibers," J. Lightwave Technol. **8**, 1799–1802 (1990).
31. Y. Li, F. Zhang, and T. Yoshino, "Wide temperature-range Brillouin and Rayleigh optical-time-domain reflectometry in a dispersion-shifted fiber," Appl. Opt. **42**, 3772–3775 (2003).
32. D. B. Leviton and J. B. Frey, "Temperature-dependent absolute refractive index measurements of synthetic fused silica," in *Proceedings of Optomechanical Technologies for Astronomy*, Orlando, FL, 2006, Vol. **6273**.
33. B. Ruffle, S. Ayrinhac, E. Courtens, R. Vacher, M. Foret, A. Wischnewski, and U. Buchenau, "Scaling the temperature-dependent Boson peak of vitreous silica with the high-frequency bulk modulus derived from Brillouin scattering data," Phys. Rev. Lett. **104**, 067402 (2010).
34. J. A. Bucaro and H. D. Dardy, "High-temperature Brillouin scattering in fused quartz," J. Appl. Phys. **45**, 5324–5329 (1974).
35. H. A. Rose, "Devitrification in annealed optical fiber," J. Lightwave Technol. **15**, 808–814 (1997).